A versatile cancer cell trapping and 1D migration assay in a microfluidic device ⓔⓟ

Colin L. Hisey ⓘⒹ, Oihane Mitxelena-Iribarren ⓘⒹ, Miguel Martínez-Calderón ⓘⒹ, Jaymeson B. Gordon ⓘⒹ, Santiago M. Olaizola, Ainara Benavente-Babace ⓘⒹ, Maite Mujika ⓘⒹ, Sergio Arana ⓘⒹ, and Derek J. Hansford ⓘⒹ

COLLECTIONS

ⓔⓟ   This paper was selected as an Editor's Pick

A versatile cancer cell trapping and 1D migration assay in a microfluidic device EP

View Online   Export Citation   CrossMark

Colin L. Hisey,[1] Oihane Mitxelena-Iribarren,[2,3] Miguel Martínez-Calderón,[2,3] Jaymeson B. Gordon,[1]
Santiago M. Olaizola,[2,3] Ainara Benavente-Babace,[4] Maite Mujika,[2,3] Sergio Arana,[2,3] and Derek J. Hansford[1,a]

AFFILIATIONS

[1]Department of Biomedical Engineering, The Ohio State University, Columbus, Ohio 43210, USA
[2]Ceit-IK4, Manuel Lardizábal 15, 20018 Donostia/San Sebastián, Spain
[3]Universidad de Navarra, Tecnun, Manuel Lardizábal 13, 20018 Donostia/San Sebastián, Spain
[4]Department of Physics, University of Ottawa, Ottawa, Ontario K1N 6N5, Canada

[a]Author to whom correspondence should be addressed: hansford.4@osu.edu

ABSTRACT

Highly migratory cancer cells often lead to metastasis and recurrence and are responsible for the high mortality rates in many cancers despite aggressive treatment. Recently, the migratory behavior of patient-derived glioblastoma multiforme cells on microtracks has shown potential in predicting the likelihood of recurrence, while at the same time, antimetastasis drugs have been developed which require simple yet relevant high-throughput screening systems. However, robust *in vitro* platforms which can reliably seed single cells and measure their migration while mimicking the physiological tumor microenvironment have not been demonstrated. In this study, we demonstrate a microfluidic device which hydrodynamically seeds single cancer cells onto stamped or femtosecond laser ablated polystyrene microtracks, promoting 1D migratory behavior due to the cells' tendency to follow topographical cues. Using time-lapse microscopy, we found that single U87 glioblastoma multiforme cells migrated more slowly on laser ablated microtracks compared to stamped microtracks of equal width and spacing ($p < 0.05$) and exhibited greater directional persistence on both 1D patterns compared to flat polystyrene ($p < 0.05$). Single-cell morphologies also differed significantly between flat and 1D patterns, with cells on 1D substrates exhibiting higher aspect ratios and less circularity ($p < 0.05$). This microfluidic platform could lead to automated quantification of single-cell migratory behavior due to the high predictability of hydrodynamic seeding and guided 1D migration, an important step to realizing the potential of microfluidic migration assays for drug screening and individualized medicine.

INTRODUCTION

The aggressive migration of individual cells is a primary contributor to low patient survival rates for many forms of cancer due to its critical role in metastasis and recurrence. The establishment of secondary tumors typically requires the successful completion of several steps, including loss of cellular adhesion, altering of and migration through the extracellular matrix (ECM), traveling through the circulatory or lymphatic system, exiting the vessel, and eventually colonizing distal tissue.[1,2] The probability of achieving these steps without being hindered by numerous protective and homeostatic mechanisms is incredibly low, such that only rare single cells will reach the final step and successfully establish a secondary tumor.[3] Many factors have been shown to influence this metastatic behavior including aspects of the cell's microenvironment such as stiffness, surface chemistry, and topography.[4–8] In glioblastoma multiforme (GBM), metastasis beyond the central nervous system is very rare, and the establishment of secondary tumors elsewhere in the brain, as well as the high incidence of recurrence due to diffuse cancer cells in the surrounding tissue, is caused by topographically guided single-cell migration on white matter tracts, blood vessels, or the subpial space. This directed migration results in dismal survival rates for nearly all patients despite aggressive treatment regimens.[9–15] To better understand and combat the underlying causes of metastasis and recurrence, many *in vitro* systems have been developed which attempt to quantify the migratory behavior of cultured cells with varying degrees of convenience, throughput, and biomimicry.[16–18]

Traditionally, cell migration analysis has been done using scratch, cell exclusion zone, or Boyden chamber-based transmembrane assays. In the scratch assay, a confluent monolayer of cells is scratched to create a gap in the cell culture on the substrate, and the rate of invasion back into the gap is quantified by measuring the position of the leading edges over time.[19,20] Cell exclusion zone assays use a similar principle, but rather than scratching the substrate to create a gap, which can be difficult to do consistently, they initially block a certain portion of the substrate from cell attachment and then remove the block and measure the invasion of cells into the gap.[21,22] In transmembrane assays, cells are seeded on one side of the membrane, while a solution to be tested for its chemotactic activity is placed on the opposing side, and the number of cells which migrate through the membrane is counted as an indication of collective migration behavior.[23,24] These types of assays provide some quantitative measure of collective cell migration and are accessible to most researchers with standard cell culture skills, but they often ignore the specific behavior of migratory single cells that break away from the primary tumor and migrate rapidly down fibrous structures. Numerous 3D matrix scaffold-based models have also been developed specifically for GBM, typically in an attempt to mimic the abundant glycoproteins and proteoglycans like hyaluronic acid in the brain ECM, as opposed to the stiffer collagen ECM matrix typically found in other organs.[25–28] Given the strong influence that the tumor microenvironment topography can have on the behavior of single cells, many biomimetic platforms specifically emphasizing the fibrous nature of the ECM have also been developed using microfabrication techniques.[29]

In an attempt to mimic the topographical guidance of single cancer cells, researchers have used aligned or randomly oriented electrospun nanofibers to mimic different tumor ECM microenvironments. For instance, aligned polycaprolactone (PCL) nanofibers have been shown to induce a more migratory phenotype in cultured GBM cells compared to flat surfaces, causing clear changes in morphology, stiffness, upregulation in genes associated with migration, and downregulation in genes associated with proliferation.[7] GBM cells cultured on aligned PCL nanofibers have also demonstrated increased sensitivity to myosin II inhibition compared to the same cells cultured on flat substrates, and migrated more rapidly and exhibited greater directional persistence on aligned PCL fibers compared to random fibers.[30,31] Lastly, by combining different polymer cores with PCL in core-shell nanofibers, GBM morphology, migration speed, focal adhesion kinase, and myosin light chain 2 expression all demonstrated a significant dependence on the properties of the fiber matrix.[32]

Recently, analysis of the underlying dimensionality of biomimetic substrates on cell migration has demonstrated that 1D topographical cues direct the migratory behavior of cells on 3D fibrous substrates, and that migration on 2D substrates differs greatly from both 1D and 3D.[33] Thus, arrays of microtracks or grooves, which have been thoroughly explored in cell attachment, proliferation, and alignment studies for decades, have returned to the spotlight due to their ease of fabrication, scalability, and capability for topographically guidance of GBM migration.[34,35] GBM cells cultured on polystyrene non-electrospun spinneret based tunable engineered parameter (STEP) fibers migrated in a single dimension when in contact with one fiber or two parallel fibers, but two dimensions

when fibers were in an orthogonal arrangement.[36] In another study, soft lithography molding was used to fabricate polystyrene microtracks, and these patterns could distinguish differences in the migratory behavior of multiple types of brain cancer.[37] A recent clinical study found that GBM recurrence was highly predictable based on the migratory behavior of single biopsied GBM cells on 1D poly(urethane-acrylate) patterns.[38]

While laser machining has been used to fabricate patterns on polystyrene which affect cell adhesion and morphology,[39] few examples exist of cell migration analysis on laser machined polymer surfaces. In one study, laser ablation was used to pattern nanoscale craters of various aspect ratios and pitches on quartz, and the patterning affected the focal-adhesion size and distribution of fibroblasts, thus affecting cell morphology, migration, and ultimately localization.[40] Further exploration of the potential clinical utility of these 1D migration substrates requires more robust *in vitro* platforms which can consistently seed single cells onto specific locations on the microfabricated tracks, eventually allowing automated and high-throughput analyses.

The ability to accurately control, precisely position, and analyze single cells has grown rapidly over the past three decades thanks to advances in micro- and nanotechnology. In particular, the advent and refinement of high-throughput single-cell trapping methodologies such as magnetic and optical tweezers, dielectrophoresis (DEP), and acoustic waves have fueled this growth.[41–43] However, some of these techniques require expensive equipment and a sufficient level of expertise and can also lead to undesired effects from the manipulated cells.[44] As a passive and more cell-friendly alternative, microfluidic hydrodynamic trapping can meet all the needs for high-throughput, precise positioning, and single-cell studies.[45] These traps have been widely used for diverse single-cell applications such as the formation of spheroids by trapping cancer cells, electrical and chemical fusion between mouse embryonic stem cells and fibroblasts, or the dynamic coflow treatment of trapped cells.[46–48] Despite the significant interest and potential clinical utility, combining this type of hydrodynamic single-cell trapping with microfabricated 1D migration substrates has not yet been demonstrated.

In this study, we demonstrate that microfabricated 1D migration substrates can be combined with microfluidic hydrodynamic traps to consistently seed single cells onto patterned polystyrene microtracks, encouraging 1D migration based on the tendency of GBM cells to follow topographical cues. Devices were first fabricated using soft lithography, spin-dewetted stamping, and femtosecond laser ablation. The migratory behavior and morphology of single U87 glioblastoma multiforme cells were then quantified using time-lapse and fluorescent microscopy. This versatile device may enhance the clinical utility of *in vitro* 1D single-cell migration assays and has potential for high-throughput and automated quantification or personalized drug screening.

MATERIALS AND METHODS

Microfluidic channel fabrication

Microchannels were fabricated using a standard soft lithography process. First, SU-8 patterns were fabricated using multilayer photolithography. SU-8 2015 negative photoresist was spin-coated

and patterned with the basic channel geometry, then an upper SU-8 2015 layer was spin-coated and the 2nd pattern layer (containing traps) was aligned to the latent image from the first exposure. Following development in SU-8 developer, wafers were treated with hexamethyldisilazane to prevent the adhesion of the PDMS during molding. Sylgard 184 PDMS was then mixed at a 10:1 ratio of base to the curing agent and poured over the SU-8 master, degassed, cured, and prepared for bonding to the polymer substrates [Fig. 1(a)]. The main channel is $600\,\mu m$ wide and 16 mm long, containing three sets of 11 traps. These three sets were spaced by 3.5 mm down the length of the channel. Within each set, each trap was spaced by $45\,\mu m$ across the width of the channel, with every other trap staggered by $100\,\mu m$ in the long axis. The specific trap design used contains a $5\,\mu m$ gap and has been described previously [Figs. 1(b)–1(e)].[46]

Substrate fabrication

10 and $15\,\mu m \times 9.95$ mm microtracks spaced by $45\,\mu m$ were fabricated via spin-dewetting and stamping using polydimethylsiloxane (PDMS) molds. SU-8 2015 masters were first patterned and developed. Following hexamethyldisilazane (HMDS) treatment, Sylgard 184 was molded as described for the channels. Once peeled from the master, partial dewetting of 10% polystyrene in anisole was performed by spin-coating at 4500 RPM for 45 s. The sacrificial dewetted layer was then stamped off onto glass slides at 170 °C with very light manual pressure ($\sim$1–2 psi), and the final features

were stamped at 170 °C with much higher manual pressure ($\sim$25–30 psi) onto standard glass slides [Figs. 2(a)–2(h)].

For laser ablated surfaces, a similar soft lithography and partial dewetting/stamping procedure was used, except a $525\,\mu m \times 9.95$ mm rectangle (slightly a smaller width than the microfluidic channel) was stamped onto standard glass slides [Fig. 2(i)]. Samples were then machined in open air atmosphere with a Ti:Sapphire laser system that generates 130 fs pulses at a central wavelength of 800 nm, with a 1 kHz repetition rate. The 8 mm diameter laser beam was focused on the samples using a $10\times$ microscope objective with a numerical aperture (NA) of 0.16 to a beam waist (ω_0) of $17\,\mu m$. A three-dimensional translational stage moved the sample under the beam with a velocity of 1.5 mm/s which resulted in 12 pulses per spot. Pulse energies of 1 and $3\,\mu J$, which correspond to laser fluencies of 0.9 and 2.7 J/cm^2, were used [Fig. 3(a)]. Three passes were performed in each groove (space between tracks) with the necessary spacing to obtain final microtrack widths of 10, 15, and $20\,\mu m$ [Fig. 3(b)].

Device assembly and 1D cell migration assay

For both stamped and laser ablated substrates, the microtracks on glass slides were manually aligned and bonded with the hydrodynamic trap microfluidic channels using oxygen plasma treatment. This activated the glass surface for bonding to PDMS as well as increased the surface energy of the polystyrene lines for protein and cell adsorption. Devices were then UV sterilized
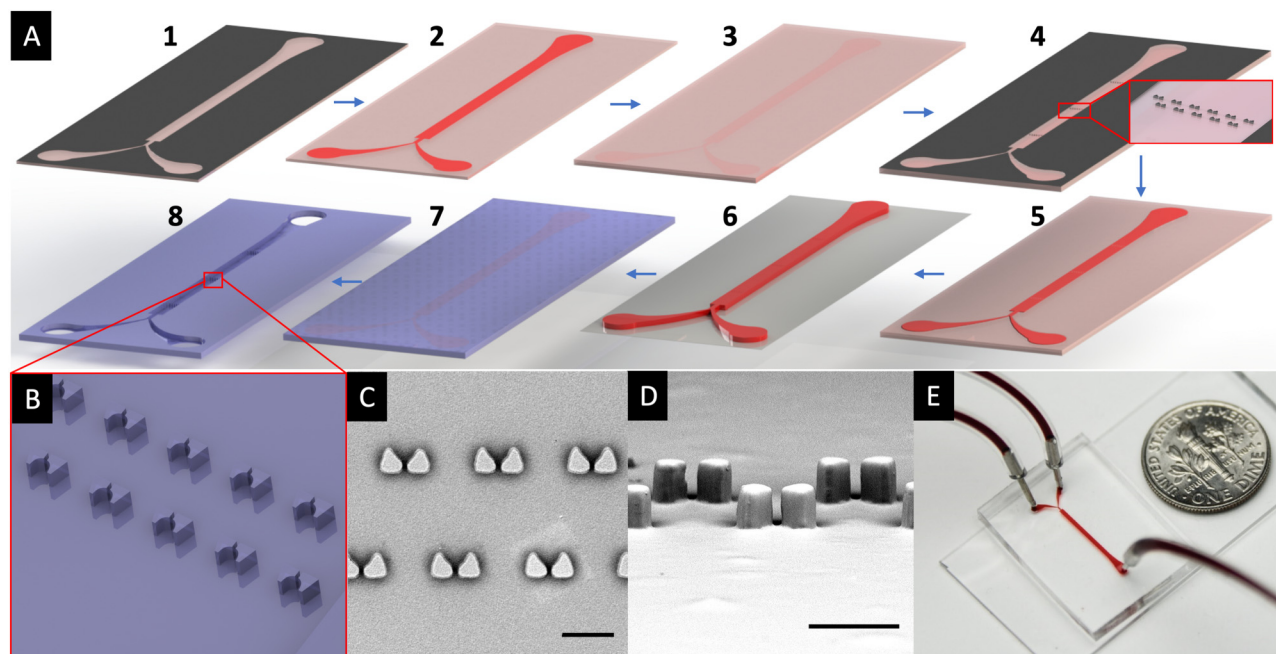

FIG. 1. Hydrodynamic trapping microfluidic channel fabrication: (a) fabrication schematic showing photolithography of first layer (1–3), second layer containing traps (4–5), development (6), soft lithography (7), and final channel with punched holes (8); (b) hydrodynamic trap design; (c) and (d) SEM images of hydrodynamic traps (bar = $50\,\mu m$); and (e) assembled device.
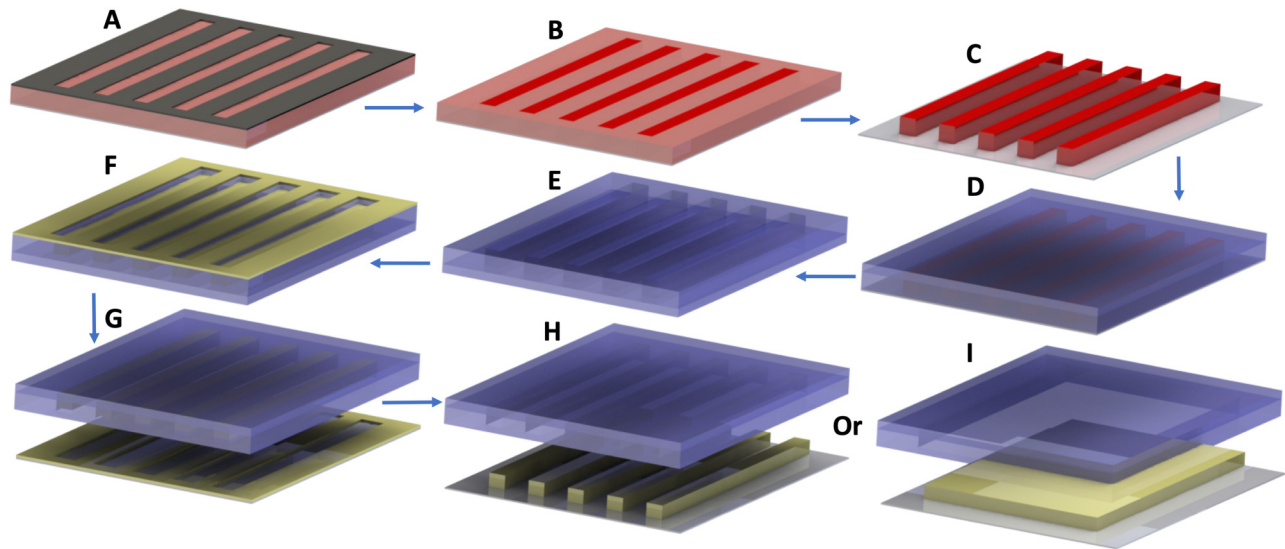
FIG. 2. Spin-dewetting microfabrication schematic with photomask (black), SU8 (red/pink), PDMS (blue) and polystyrene (yellow): photolithography (a)–(c), soft lithography, and spin-dewetting (d)–(f), stamping off dewetted layer (g), and final stamp of lines, (h) or channel-wide rectangle, if a rectangle mask was used (i).

overnight, and before introducing the cell suspension, the devices were pretreated with Minimum Essential Medium (MEM) + 10% Fetal Bovine Serum (FBS) + 1% penicillin/streptomycin for 3 h to allow for the passive adsorption of serum proteins and to mimic standard cell culture conditions. U87 glioblastoma multiforme cells (Sigma) were seeded at a concentration of 10^5 cells/ml in the same culture medium at low flow rates (<3 μl/min) to minimize damage from shear forces. Once the trapping of single cells was visually

confirmed and the remaining cell suspension had passed through the channel, flow was paused and cells were allowed to adhere to the underlying microtrack substrate for ~2 h, then the flow was reversed and set to 50 nl/min to encourage cells to migrate out and away from the traps and maintain fresh culture media throughout the duration of the migration. Images were captured every 10 min for 24 h using a Nikon Eclipse Ti time-lapse microscope (Nikon Instruments, Inc.), maintaining 5% CO_2, 37 °C, and high humidity for the duration of
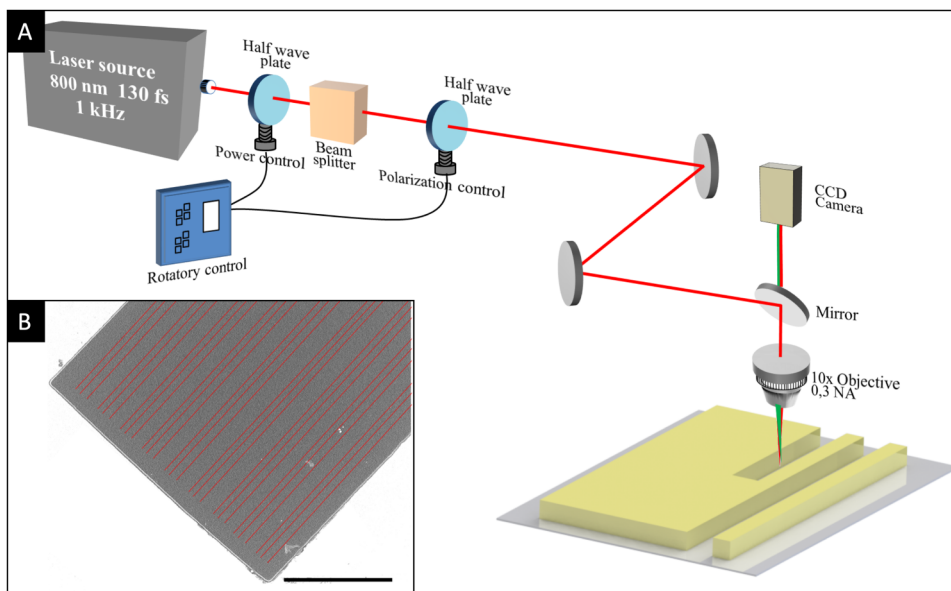

FIG. 3. Femtosecond laser ablated microfabrication schematic: (a) laser setup and (b) ablation path drawn over an SEM image of a stamped polystyrene rectangle [from Fig. 2(i), bar = 200 μm].

the assay. The manual tracking plugin in FIJI was used to quantify cell's migratory behavior.

Scanning electron microscopy and profilometry

Scanning Electron Microscopy (SEM) was performed using a Phenom G2 Pro (Phenom World) to qualitatively assess the stamped and laser ablated substrates as well as microfluidic channel structures. Profilometry was performed using a P6 Stylus profilometer (KLA Tencor) to determine the vertical profile of the microtracks.

Cell morphology and immunofluorescence analysis

Cell morphology (area, perimeter, circularity, and aspect ratio) was quantified by manually tracing cells using FIJI. First, U87 cells were bulk seeded at 25 000 cells/ml onto the polystyrene microtracks without the use of microfluidic channels and allowed to adhere for 24 h. Immunofluorescence microscopy was then performed by fixing cells with 4% paraformaldehyde and then staining with three separate reagents: 4′,6-diamidino-2-phenylindole (DAPI) for the nuclei, TRITC-phalloidin for the actin filaments, and antivinculin followed by FITC-IgG for the focal adhesions (EMD Millipore). The unsharp mask filter in FIJI as well as brightness/contrast tools were used to better visualize the cell structure before merging the channels.

STATISTICAL ANALYSIS

Unpaired t-test, one-way ANOVA, and Tukey-HSD multi-comparison tests were performed for all datasets in MATLAB or Graphpad Prism ($\alpha = 0.05$). Results are reported as averages ± standard error of the mean, and error bars are the standard error of the mean.
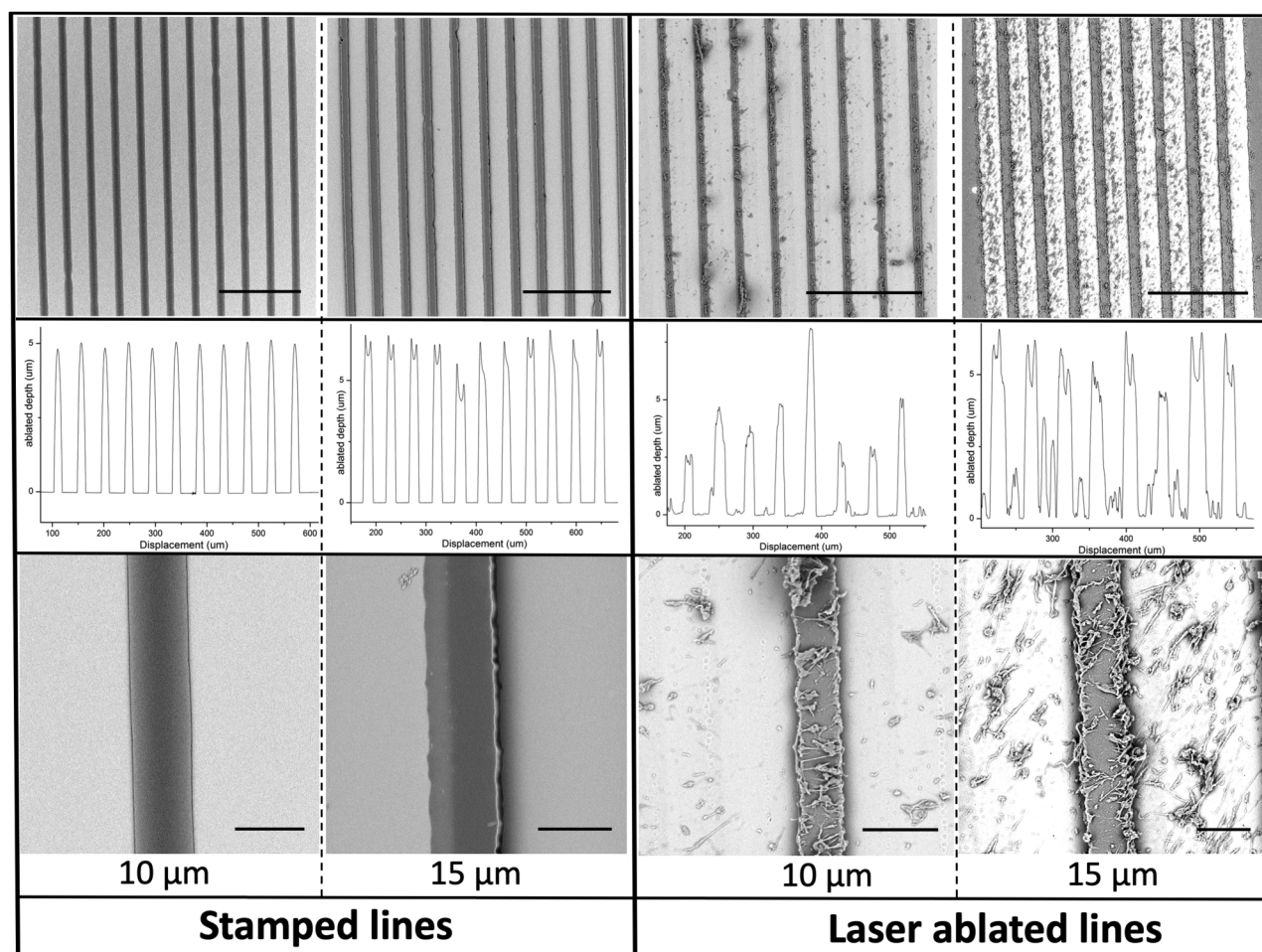

FIG. 4. Stamped compared to femtosecond laser ablated polystyrene lines: (top) SEM images of a channel-wide polystyrene line array (bar = 150 μm), (middle) profilometry, and (bottom) SEM images showing increased micro- and nanotopography created from ablation debris compared to smoother stamped microtracks (bar = 15 μm).

RESULTS AND DISCUSSION

Substrate fabrication and device assembly

The microtracks fabricated by stamping and femtosecond laser ablation showed noticeable topographical differences. Stamped microtracks exhibited much smoother surface features and consistent topography, while laser ablated microtracks exhibited much higher surface roughness and presumably surface energy due to the debris that deposits as the polystyrene is ablated (Fig. 4). Microtracks on glass substrates produced from both fabrication methods were successfully aligned and irreversibly bonded to PDMS microchannels with embedded hydrodynamic traps. The stamped microtracks displayed a slight lateral displacement to the traps due to the applied pressure and thermal expansion during the final pattern transfer, whereas the laser ablated microtracks aligned perfectly with the embedded traps across the entire channel. In future designs, this thermal expansion displacement could be calculated and compensated for in the mask design. In addition, the stamped microtracks were much easier to fabricate rapidly as the slope of the ablation path is needed to be aligned with each flat polystyrene base for the full length of the channel. Because the polystyrene film was ablated down to the glass surface, independent rather than interconnected microtracks were stamped to provide an accurate comparison between fabrication methods.

For this initial study, $10\,\mu m$ microtracks with the same spacing as the traps ($45\,\mu m$) were chosen to demonstrate that each individual track could be aligned within a few micrometers of each microfluidic trap using manual alignment [Figs. 5(a) and 5(d)]. Depending on the application, many other patterns with different track widths or spacing could be used to either encourage or prevent cell-to-cell contact or limit the number of tracks with which a cell comes in contact. GBM morphology and migration speed have been shown to be faster and more directionally persistent in 1D geometries compared to 2D, with a greater speed while in contact with parallel fibers compared to single fibers.[36] In our device, cells most often moved into the grooves between the polystyrene microtracks and remained in contact with parallel polystyrene tracks throughout the course of their migration, but the spacing could easily be adjusted to encourage a single track behavior as well.

Cell trapping and migration

Cell migration analysis indicated clear differences between U87 migration on flat, $10\,\mu m$ stamped, and $10\,\mu m$ laser ablated polystyrene substrates [Figs. 5(e) and 5(f)]. Cell migration speed, calculated as the total distance traveled over time, demonstrated that U87 cells migrated more quickly on $10\,\mu m$ stamped compared to $10\,\mu m$ laser ablated microtracks, with average migration speeds of 54.85 ± 2.21 and $37.21 \pm 4.44\,\mu m/h$ [Fig. 5(b), $p < 0.05$]. We hypothesize that the slower migration speed on the laser ablated surface could be due to an increase in the focal adhesion formation on the high surface energy debris scattered across the surface during the machining process. Based on previous studies, slower
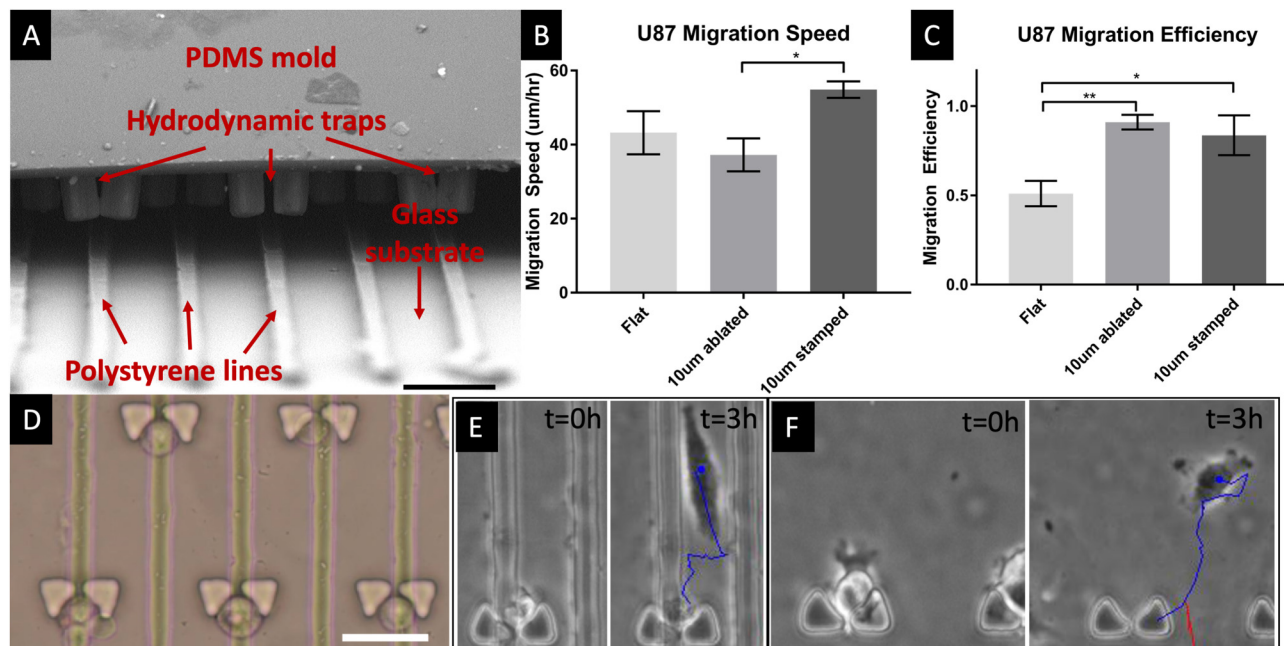

FIG. 5. Device assembly and cell migration results: (a) SEM image of the cross section of an assembled device with hydrodynamic traps aligned over $10\,\mu m$ lines (bar = $50\,\mu m$); (b) U87 migration speed; (c) U87 migration efficiency comparison; (d) seeded cells showing both single cells and one cell cluster (bar = $50\,\mu m$); (e) U87 migration example on stamped polystyrene lines; and (f) U87 migration example on flat polystyrene.
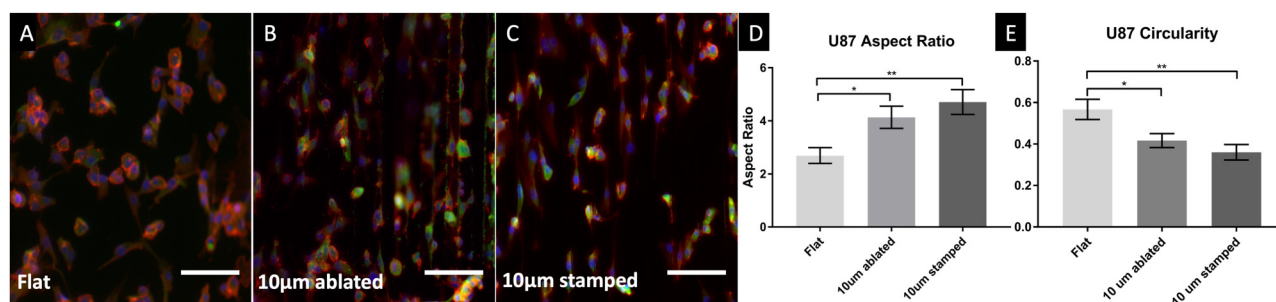
FIG. 6. Cell morphology and immunofluorescence images of U87 cells on (a) flat polystyrene, (b) $10\,\mu m$ laser ablated lines, and (c) $10\,\mu m$ stamped lines (bar = $100\,\mu m$). Comparison of the U87 morphology including (d) aspect ratio and (e) circularity.

migration was expected on flat polystyrene,[33] but surprisingly, no significant difference was found between flat polystyrene and the 1D system ($p = 0.17$ vs stamped and $p = 0.61$ vs ablated lines), likely due to the large variance exhibited by the cells. This variance could be due to the lack of organized topographical cues to provide migration stimuli, the cell interaction with the PDMS traps, or simply the generally high migration rate of U87 cells.

Cell directional persistence, sometimes referred to as migration efficiency, is the ratio of the net displacement to the trajectory path, and a clear difference was measured between the U87 cell migration on flat compared to stamped and laser ablated polystyrene microtracks, with average efficiencies of 0.51 ± 0.07, 0.83 ± 0.11, and 0.91 ± 0.04, respectively [Fig. 5(c), $p < 0.01$]. Furthermore, there was no significant difference seen between the migration efficiencies of U87 cells on the patterned substrates, with both patterns resulting in high directional persistence. Together, these differences further emphasize the importance of quantifying the migratory behavior of single GBM cells on patterned rather than flat substrates due to the high directional persistence and more consistent migration velocity.

Cell morphology

The cytoskeletal structure, nuclei location, and focal adhesions were immunofluorescently labeled and examined for qualitative comparison. As expected, U87 cells on microtracks appeared to exhibit more aligned actin filaments and terminally located nuclei [Figs. 6(a)–6(c)]. Cell morphology analysis was performed by manually tracing phase contrast images of single U87 cells, or those which were not clearly in contact with other cells, on the various substrates using FIJI. Area, perimeter, aspect ratio, and circularity were analyzed, and significant differences were found in aspect ratio and circularity. No significant differences were found between the area and the perimeter of U87 cells on various substrates. The aspect ratios, or the ratio of long to short axes, of U87 cells on $10\,\mu m$ stamped and laser ablated polystyrene microtracks were greater than flat polystyrene, with average values of 4.71 ± 0.47, 4.13 ± 0.42, and 2.69 ± 0.30, respectively [Fig. 6(d), $p < 0.05$], with a greater aspect ratio corresponding to the more aligned actin filaments. Cell circularity was calculated using Eq. (1), with a value

of 1.0 indicating a perfect circle,

$$\text{Circularity} = 4\pi \times \frac{\text{Area}}{\text{Perimeter}^2}. \qquad (1)$$

Significantly greater circularity was found for U87 cells on flat polystyrene compared to both ablated and stamped substrates, with average values of 0.56 ± 0.05, 0.42 ± 0.03, and 0.36 ± 0.03 [Fig. 6(e), $p < 0.01$]. Together, this morphology analysis indicates the degree to which the cells respond to the topographical cues. In the future, this analysis could be performed using a fluorescence microscopy and a live cell stain such as calcein to more easily automate the process and minimize potential biases.

CONCLUSIONS

In this study, we demonstrate that hydrodynamic trapping can be combined with stamped and femtosecond laser ablated polystyrene microtracks in a microfluidic device to create a versatile platform for characterizing single cancer cell migration. By consistently seeding single cells in known starting locations and encouraging directional persistence via topographical cues, we can improve the reproducibility and physiological relevance of many conventional assays. In addition, the fabrication methods used can be easily adjusted to incorporate a variety of other polymers, patterns, or adhesion proteins to model various *in vivo* tissues with a range of surface chemistries, stiffnesses, or topographies. This device will aid in current efforts to automate the quantification of single cancer cell migration behavior for use as a predictor of patient outcomes or in antimetastasis drug screening.

ACKNOWLEDGMENTS

REFERENCES

[1]A. F. Chambers, A. C. Groom, and I. C. MacDonald, Nat. Rev. Cancer **2**(8), 563–572 (2002).

[2]I. Fidler, Nat. Rev. Cancer **3**, 453–458 (2003).

[3]G. P. Gupta and J. Massague, Cell **127**(4), 679–695 (2006).

[4]P. Friedl and S. Alexander, Cell **147**(5), 992–1009 (2011).

[5]T. Ohnishi, S. Hiraga, S. Izumoto, H. Matsumura, Y. Kanemura, N. Arita, and T. Hayakawa, Clin. Exp. Metastasis **16**(8), 729–741 (1998).

[6]T. A. Ulrich, E. M. de Juan Pardo, and S. Kumar, Cancer Res. **69**(10), 4167–4174 (2009).

[7]A. Beliveau, G. Thomas, J. Gong, Q. Wen, and A. Jain, Sci. Rep. **6**, 26143 (2016).

[8]A. Giese, M. Rief, M. Loo, and M. Berens, Cancer Res. **54**(14), 3897–3904 (1994).

[9]V. A. Cuddapah, S. Robel, S. Watkins, and H. Sontheimer, Nat. Rev. Neurosci. **15**(7), 455–465 (2014).

[10]D. Louis, Annu. Rev. Pathol. Mech. Dis. **1**, 97–117 (2006).

[11]E. Holland, Proc. Natl. Acad. Sci. U.S.A. **97**(12), 6242–6244 (2000).

[12]A. C. Bellail, S. B. Hunter, D. J. Brat, C. Tan, and E. G. Van Meir, Int. J. Biochem. Cell Biol. **36**(6), 1046–1069 (2004).

[13]P. Y. Wen and S. Kesari, New Engl. J. Med. **359**(5), 492–507 (2008).

[14]P. G. Gritsenko, O. Ilina, and P. Friedl, J. Pathol. **226**(2), 185–199 (2012).

[15]A. Giese and M. Westphal, Neurosurgery **39**(2), 235–250 (1996).

[16]N. Kramer, A. Walzl, C. Unger, M. Rosner, G. Krupitza, M. Hengstschlager, and H. Dolznig, Mutat. Res. **752**(1), 10–24 (2013).

[17]K. I. Hulkower and R. L. Herber, Pharmaceutics **3**(1), 107–124 (2011).

[18]W. Xiao, A. Sohrabi, and S. Seidlits, Future Sci. OA **3**(3), FSO189 (2017).

[19]E. Kim, H. Song, S. Yoo, and M. Yoon, Oncotarget **7**(40), 65125–65136 (2016).

[20]S. H. Ahn, H. Park, Y. H. Ahn, S. Kim, M. S. Cho, J. L. Kang, and Y. H. Choi, Sci. Rep. **6**, 24552 (2016).

[21]Y. Kam, C. Guess, L. Estrada, B. Weidow, and V. Quaranta, BMC Cancer **8**, 198 (2008).

[22]M. Poujade, E. Grasland-Mongrain, A. Hertzog, J. Jouanneau, P. Chavrier, B. Ladoux, A. Buguin, and P. Silberzan, Proc. Natl. Acad. Sci. U.S.A. **104**(41), 15988–15993 (2007).

[23]H. Kim, H. S. Roh, J. E. Kim, S. D. Park, W. H. Park, and J. Y. Moon, Nutr. Res. Pract. **10**(3), 259–264 (2016).

[24]K. Kobayashi, H. Takahashi, A. Inoue, H. Harada, S. Toshimori, Y. Kobayashi, K. Goto, K. Sugimoto, H. Yano, T. Ohnishi, and J. Tanaka, J. Cell. Biochem. **113**(2), 508–517 (2012).

[25]Y. Kim and S. Kumar, Mol. Cancer Res. **12**(10), 1416–1429 (2014).

[26]L. W. Lau, R. Cua, M. B. Keough, S. Haylock-Jacobs, and V. W. Yong, Nat. Rev. Neurosci. **14**(10), 722–729 (2013).

[27]J. Cha and P. Kim, Front. Mater. **4**, 45 (2017).

[28]J. Cha, S. G. Kang, and P. Kim, Sci. Rep. **6**, 24912 (2016).

[29]S. S. Rao, J. J. Lannutti, M. S. Viapiano, A. Sarkar, and J. O. Winter, Tissue Eng. Part B Rev. **20**(4), 314–327 (2014).

[30]P. A. Agudelo-Garcia, J. K. De Jesus, S. P. Williams, M. O. Nowicki, E. A. Chiocca, S. Liyanarachchi, P.-K. Li, J. J. Lannutti, J. K. Johnson, S. E. Lawler, and M. S. Viapiano, Neoplasia **13**(9), 831 (2011).

[31]J. Johnson, M. O. Nowicki, C. H. Lee, E. A. Chiocca, M. S. Viapiano, S. E. Lawler, and J. J. Lannutti, Tissue Eng. Part C **15**(4), 531–540 (2009).

[32]S. S. Rao, M. T. Nelson, R. Xue, J. K. DeJesus, M. S. Viapiano, J. J. Lannutti, A. Sarkar, and J. O. Winter, Biomaterials **34**(21), 5181–5190 (2013).

[33]A. D. Doyle, F. W. Wang, K. Matsumoto, and K. M. Yamada, J. Cell Biol. **184**(4), 481–490 (2009).

[34]J. Cha, I. Koh, Y. Choi, J. Lee, C. Choi, and P. Kim, Adv. Healthcare Mater. **4**(3), 405–411 (2015).

[35]W. Sim, J. Cha, J. Choi, and K. Choi, Biotechnol. Bioprocess Eng. **22**(2), 107–113 (2017).

[36]H. M. Estabridis, A. Jana, A. Nain, and D. J. Odde, Ann. Biomed. Eng. **46**(3), 392–403 (2018).

[37]D. Gallego-Perez, N. Higuita-Castro, L. Denning, J. DeJesus, K. Dahl, A. Sarkar, and D. J. Hansford, Lab Chip **12**(21), 4424–4432 (2012).

[38]C. L. Smith, O. Kilic, P. Schiapparelli, H. Guerrero-Cazares, D. H. Kim, N. I. Sedora-Roman, S. Gupta, T. O'Donnell, K. L. Chaichana, F. J. Rodriguez, S. Abbadi, J. Park, A. Quinones-Hinojosa, and A. Levchenko, Cell Rep. **15**(12), 2616–2624 (2016).

[39]B. Zhu, Q. Zhang, Q. Lu, Y. Xu, J. Yin, J. Hu, and Z. Wang, Biomaterials **25**(18), 4215–4223 (2004).

[40]H. Jeon, S. Koo, W. M. Reese, P. Loskill, C. P. Grigoropoulos, and K. E. Healy, Nat. Mater. **14**(9), 918–923 (2015).

[41]A. Chen, T. Byvank, W. Chang, A. Bharde, G. Vieira, B. Miller, J. Chalmers, R. Bashir, and R. Sooryakumar, Lab Chip **13**(6), 1172–1181 (2013).

[42]H. Andersson and A. van den Berg, Curr. Opin. Biotechnol. **15**(1), 44–49 (2004).

[43]J. Voldman, Annu. Rev. Biomed. Eng. **8**, 425–454 (2006).

[44]D. Carlo and L. Lee, Anal. Chem. **78**(23), 7918–7925 (2006).

[45]M. Tanyeri and C. M. Schroeder, Nano Lett. **13**(6), 2357–2364 (2013).

[46]A. Benavente-Babace, D. Gallego-Perez, D. J. Hansford, S. Arana, E. Perez-Lorenzo, and M. Mujika, Biosens. Bioelectron. **61**, 298–305 (2014).

[47]L. Y. Wu, D. Di Carlo, and L. P. Lee, Biomed. Microdevices **10**(2), 197–202 (2008).

[48]A. M. Skelley, O. Kirak, H. Suh, R. Jaenisch, and J. Voldman, Nat. Methods **6**(2), 147–152 (2009).